Additional data for

Dynamic Partitioning of a GPI-Anchored Protein in Glycosphingolipid-Rich Microdomains Imaged by Single-Quantum Dot Tracking

Fabien Pinaud[1,3], Xavier Michalet[1,3], Gopal Iyer[1], Emmanuel Margeat[1], Hsiao-Ping Moore[2], Shimon Weiss[1,3].

[1]Department of Chemistry & Biochemistry, University of California, Los Angeles, CA, USA.
[2]Department of Molecular & Cell Biology, University of California, Berkeley, CA, USA.

[3]Corresponding authors:
fabien.pinaud@lkb.ens.fr; michalet@chem.ucla.edu and sweiss@chem.ucla.edu

Published in Traffic ……..

Note: The following additional data are part of the supplementary information that were submitted and reviewed for publication of the manuscript in Traffic. Unfortunately, because of size constrains, these additional data could not be posted together with the rest of the supplementary information on Traffic website.

These data include:

Single-molecule dual-color total internal reflection fluorescence (TIRF) microscopy setups

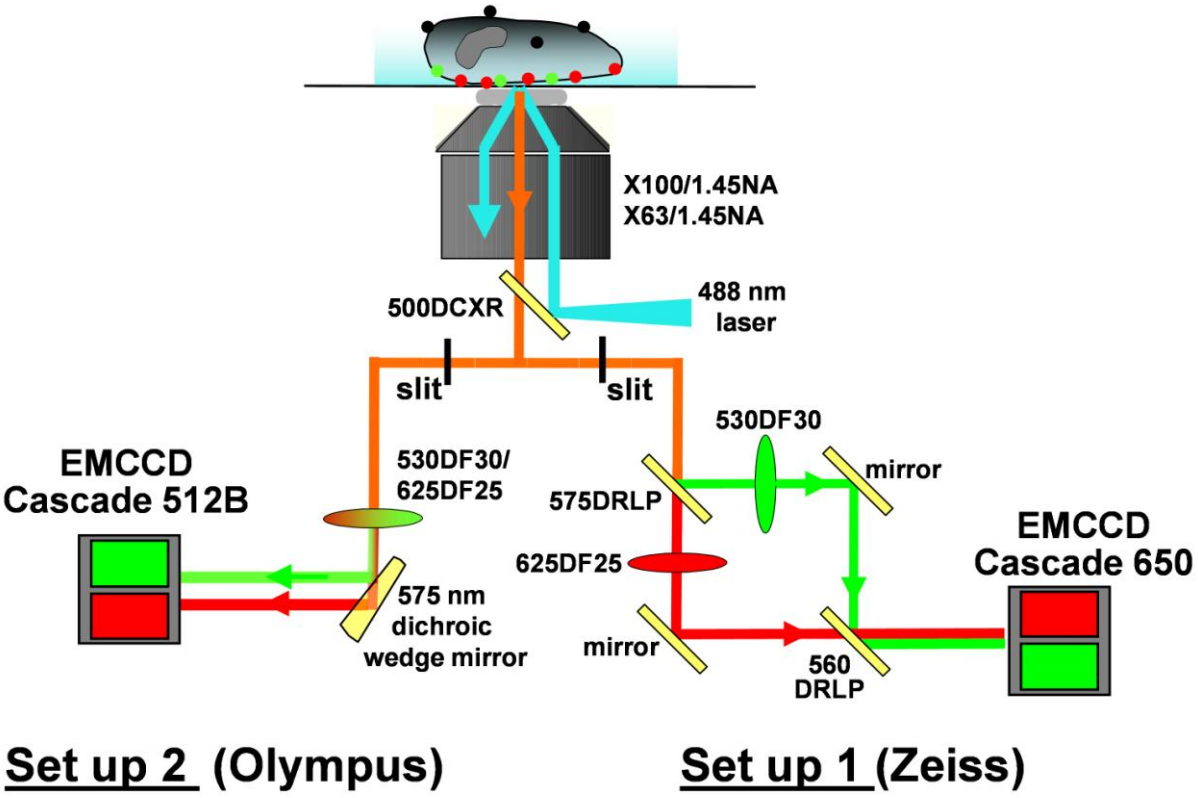

Crosslinking of Av-GPI induces patches in the absence of CTxB

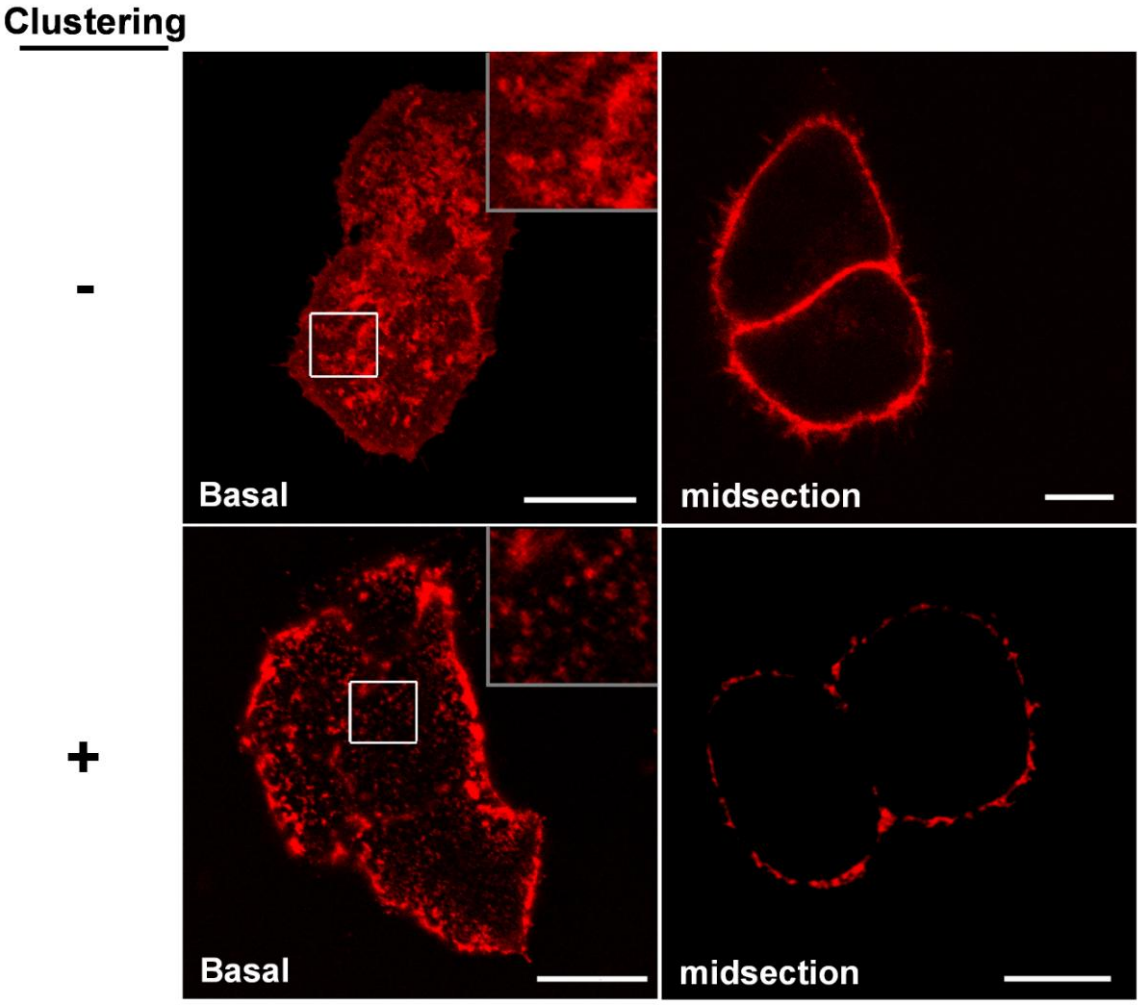

Av-GPI expressing HeLa cells were labeled with Alexa-594 biocytin (-, top panels) or incubated with biotinylated anti-avidin antibodies and further labeled with Texas Red avidin (+, bottom panels) to induce clustering of Av-GPI at 12 ºC. Confocal images at the ventral membrane or at midsections of cells show the redistribution of Av-GPI into clusters upon cross-linking. These clusters colocalized with GM1-rich domains when labeled Alexa 488 CTxB (see Figure 1). Inserts are zoomed-in images of the delineated regions. Scale bars: basal 20 µm, midsection 10 µm.

Comparison between single-trajectory PDSD analysis and global PDSD analysis

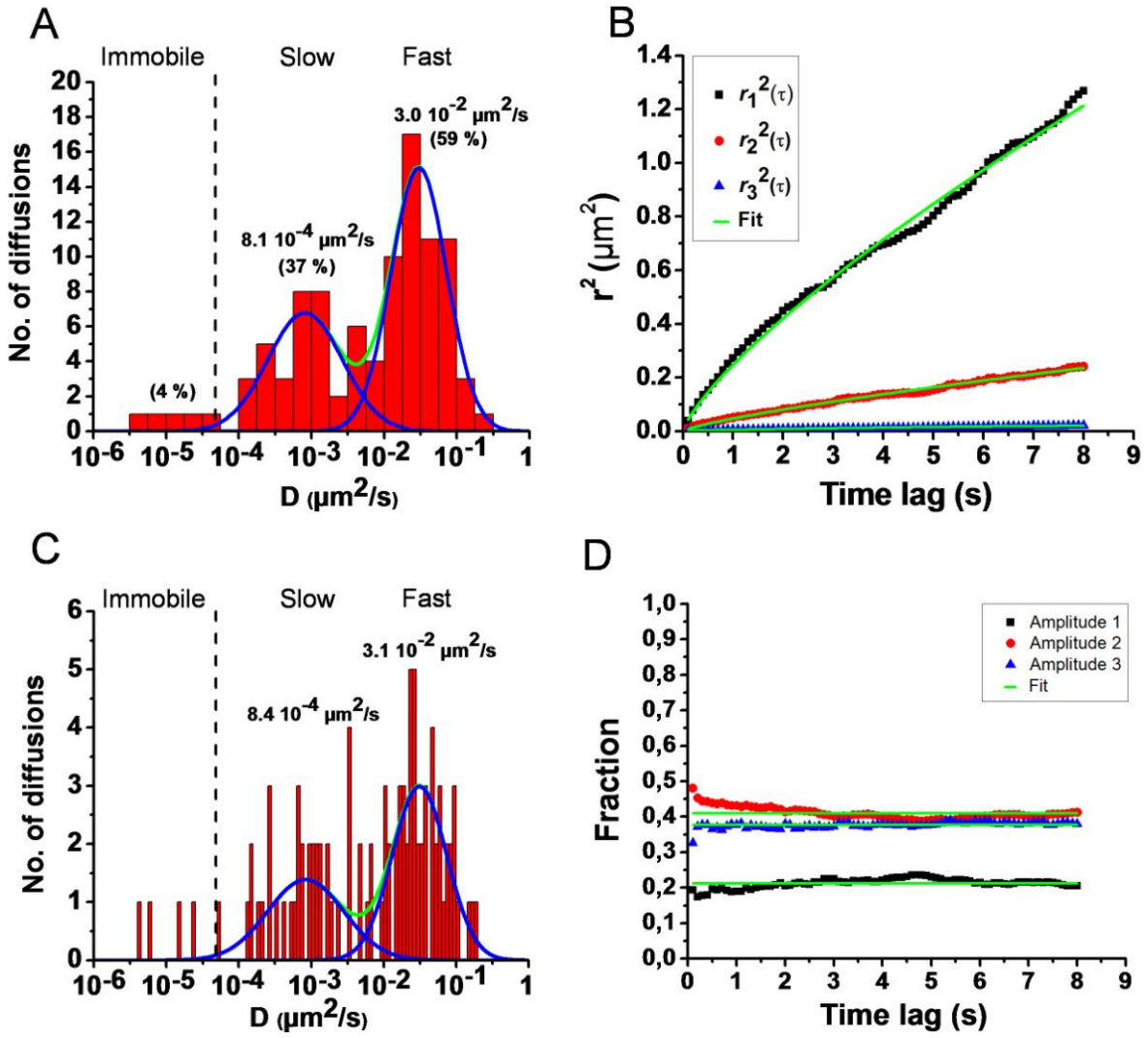

(A) Distribution of diffusion coefficients after PDSD analysis of 71 individual trajectories of Av-GPI labeled with quasi-monovalent biotinylated qdots. 59 % of Av-GPI diffusions are classified as fast with $\hat{D}_{fast}^{pauci}$ = 3.0 10^{-2} µm^2/s (SE: 2.5-3.6 10^{-2} µm^2/s) while 37 % are classified as slow with $\hat{D}_{slow}^{pauci}$ = 8.1 10^{-4} µm^2/s (SE: 0.6-1.1 10^{-3} µm^2/s). 4 % of the GPI-test probes were immobile. The width of the distribution was taken into account to optimize the histogram bin (see Material and Methods).

(B) Global PDSD analysis of the same 71 Av-GPI traces pooled together. The global PDSD curves could be described with a minimum of three fitting exponents. Note that, owing to the wide bimodal log-normal distribution of diffusion coefficients in (A) it is not surprising that that a minimum of three *average* diffusion regimes is required to account for the *ensemble* behavior. The three $r_i^2(t)$ curves recovered were well fitted with anomalous diffusion models $\langle r^2 \rangle = 4D_\alpha t^\alpha$ with α_1 of 0.76, α_2 of 0.77 and α_3 of 0.67 and $D_{\alpha 1}$ = 6.2 10^{-2}, $D_{\alpha 2}$ = 1.2 10^{-2} and $D_{\alpha 3}$ = 1.3 10^{-3} µm^2/s, for r_1^2(t), r_2^2(t) and r_3^2(t) respectively. Heterogeneous diffusion within the fast and slow sub-populations may explain the appearance of this third sub-diffusion as well as the anomalous diffusive behaviors. Notice that a direct comparison between diffusion values evaluated from single trajectories PDSD in (A) with the results of the global PDSD analysis is difficult, notably because the diffusions from global analysis are time dependent, and the values determined in (A) involved traces of different duration (mean trajectory duration 83.6 ± 25.3 s). For the sake of comparing both sets of data we give here the calculated diffusion coefficients for a time interval t = 8.0 s corresponding to ~10 % of the mean duration of all trajectories: $D_{ens,1}$ = 3.8 10^{-2} µm^2/s; $D_{ens,2}$ = 6.4 10^{-4} µm^2/s and $D_{ens,3}$ = 7.3 10^{-3} µm^2/s. While $D_{ens,1}$ and $D_{ens,2}$ compare well with the modal values $\hat{D}_{fast}$ and $\hat{D}_{slow}$ of the fast

and slow sub-populations obtained from single-trajectory analysis in (A), $D_{ens,3}$ appears intermediate. These results illustrate the oversimplified (yet consistent) picture provided by the ensemble analysis compared to the wealth of information obtained in the single-trajectory analysis.
(C) Distribution of diffusion coefficients as in (A) but with a 5 times smaller bin size. Plot of the distribution with a small bin size was performed to check whether a third diffusing population was hidden within the width of the fast or slow population. This does not seem to be the case. This underlines that the third and intermediate sub-population detected by global PDSD analysis in (B) most likely arises from the broad distribution of these two main sub-populations.
(D) Fractions of the three sub-populations detected by global PDSD analysis in (B). The amplitudes of the fit on PDSD curves are plotted as a function of time lags. Fractions were 21 %, 38 % and 41 %, for $D_{ens,1,}$ $D_{ens,2}$ and $D_{ens,3}$ respectively. Notice that the combined fraction of $D_{ens,1}$ and $D_{ens,3}$ (62 %) corresponds well to the fraction of that determined for the fast diffusing sub-population in (A) while the fraction of $D_{ens,2}$ is in good agreement with that of slow sub-diffusions in (A). This implies that the third sub-population detected might arise from the distribution width of the fast Av-GPI sub-population.

Distribution of Av-GPI diffusion coefficients in untreated HeLa cells at 37°C

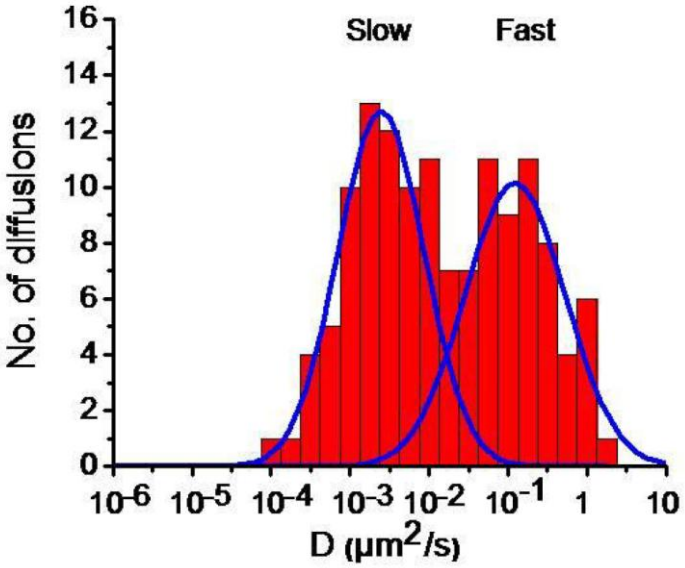

PDSD analysis of 84 Av-GPI tracked on 9 HeLa cells at 37°C. Two diffusion population of Av-GPI were still detected. Slow Av-GPI diffused at 2.5 10^{-3} µm^2/s (SE 1.7-6.7 10^{-3} µm^2/s, 43 %) while the fast population diffused at 1.2 10^{-1} µm^2/s (SE 0.75-2.0 10^{-1} µm^2/s, 57 %). Among the 84 Av-GPI, 46 % had a single diffusion regime (and diffusion coefficient), while 51 % exhibited two diffusion regimes and 3 % exhibited three diffusion regimes. 29 % of all trajectories switched between the fast and slow diffusion regime (or vice versa) during tracking. Both slow and fast regimes for Av-GPI diffuse more rapidly at 37°C than at room temperature (RT) with a ~40-fold difference in their apparent diffusion coefficients. As previously observed by FRAP (Fig. S1), the increase in diffusion coefficient is about 3-fold. The respective fraction of slow (43% at 37°C *vs.* 42% at room temp.) and fast diffusion (57% at 37°C *vs.* 55% at RT) is also unchanged when measurement is done at 37°C rather than at RT. Notice that it is not surprising to detect a higher percentage of Av-GPI with 2 or more diffusion regimes at 37°C (54% at 37°C *vs.* 34% at RT), as well as a higher percentage of Av-GPI switching from the fast to slow diffusion regime (29% at 37°C *vs.* 22% at RT). Because Av-GPI diffuse faster, there is a higher probability to detect events where Av-GPI change diffusion, for a finite observation time similar to that used when imaging at room temperature. These observations confirm that working at RT did not significantly affect the membrane properties in HeLa cells.

Visualization of slow/immobile molecules using mean intensity projection images

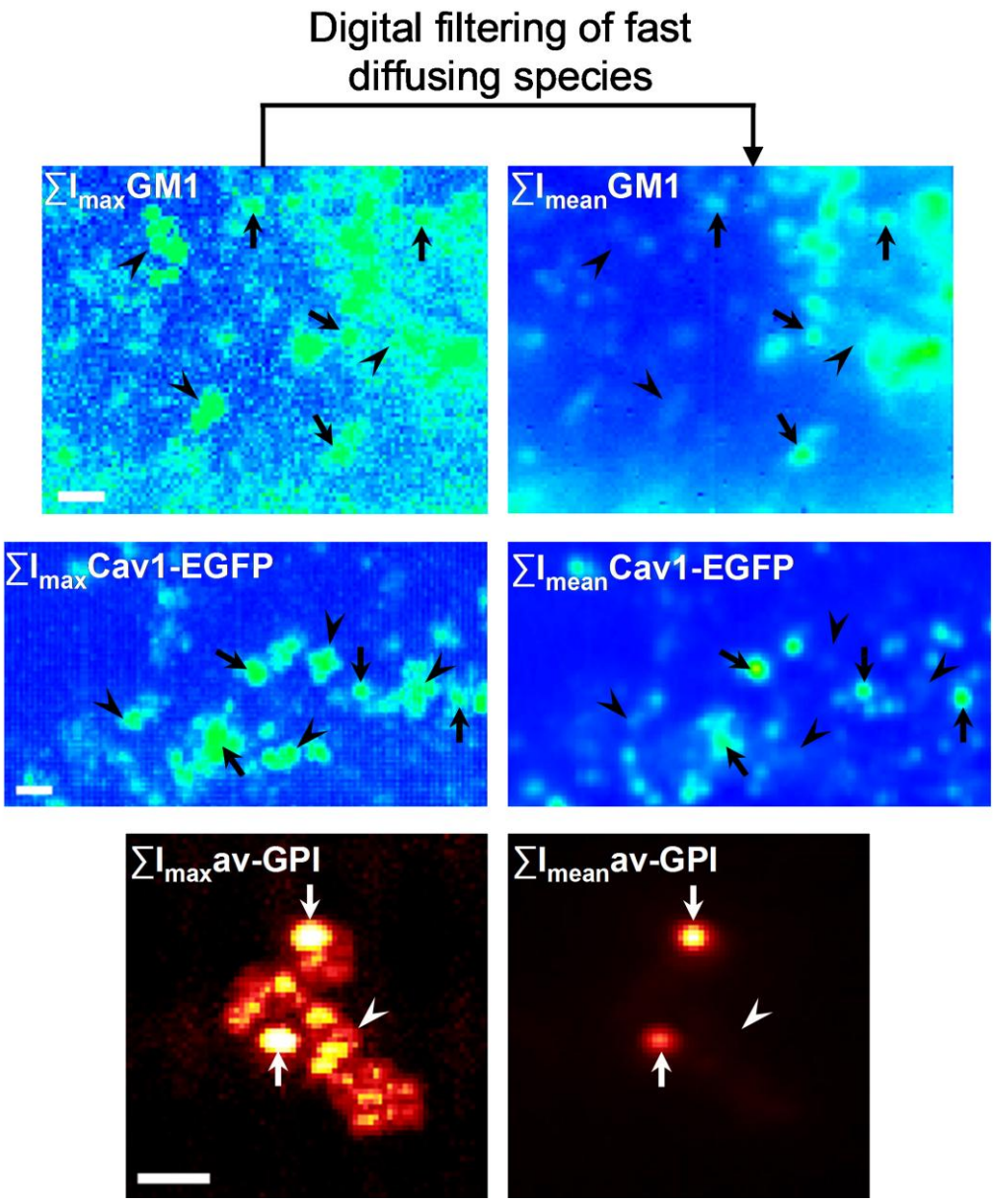

A comparison between a pixel-based maximum intensity projection image ($\sum I_{max}$, left panels) and the corresponding average intensity projection image ($\sum I_{mean}$, right panels) for all frames of a movie is presented for CTxB-labeled GM1 domains (top), Cav1-EGFP (middle) and qdot labeled Av-GPI (bottom). While $\sum I_{max}$ permits the visualization of all the fast diffusing (arrow heads) and slow/immobile (arrows) CTxB, Cav1-EGFP and Av-GPI molecules in the entire movie, $\sum I_{mean}$ allows the digital filtering out of fast diffusing species, which do not appear in the final image. With this filtering, membrane domains with slow diffusion can be easily identified during the entire movie, despite fast photobleaching of the fluorophores.

Immunostaining of endogenous caveolin-1 and colocalization with caveolin-1-EGFP in two HeLa cell lines

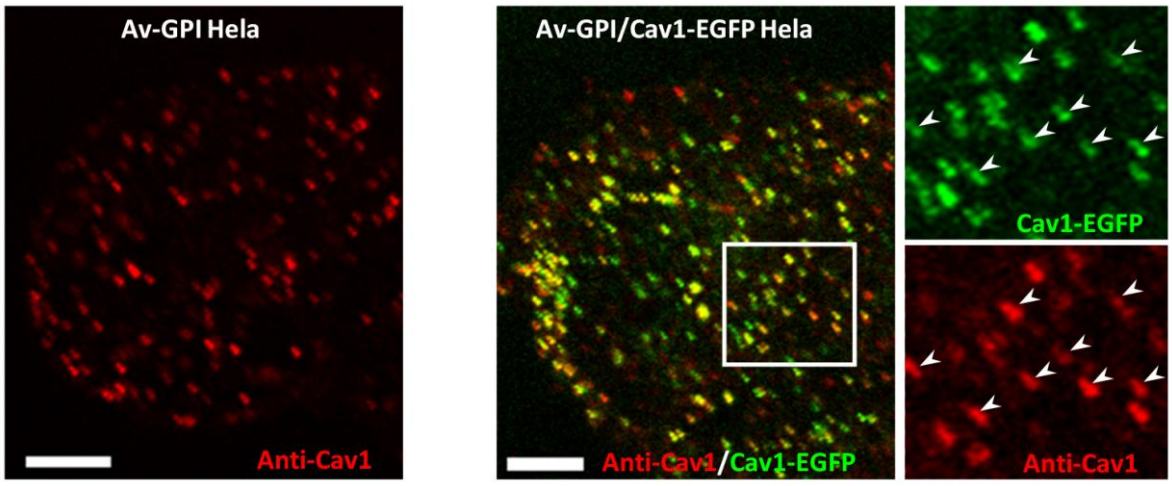

Indirect immunostaining of membrane caveolae in HeLa cell expressing Av-GPI only (left panel) or co-expressing Av-GPI and Cav1-EGFP (right panels). A specific N-20 antibody against the caveolar form of caveolin-1 was used to image both endogenous and Cav1-EGFP labeled caveoale at the ventral plasma membrane. The higher staining density in Av-GPI/Cav1-EGFP cells indicates that expression of Cav1-EGFP results in an increased amount of caveolae in the membrane of these cells compared to HeLa expressing Av-GPI only. Colocalization between anti-caveolin-1 antibodies and Cav1-EGFP also shows that a large majority of caveolae are labeled with the fluorescent protein fusion. A magnified region of interest (ROI, white square) shows the frequent colocalization (arrows) between Cav1-EGFP and anti-caveolin-1 antibodies. Scale bars: 5 µm.

Quantification of Av-GPI membrane expression in Av-GPI and Av-GPI/Cav1-EGFP expressing HeLa cells

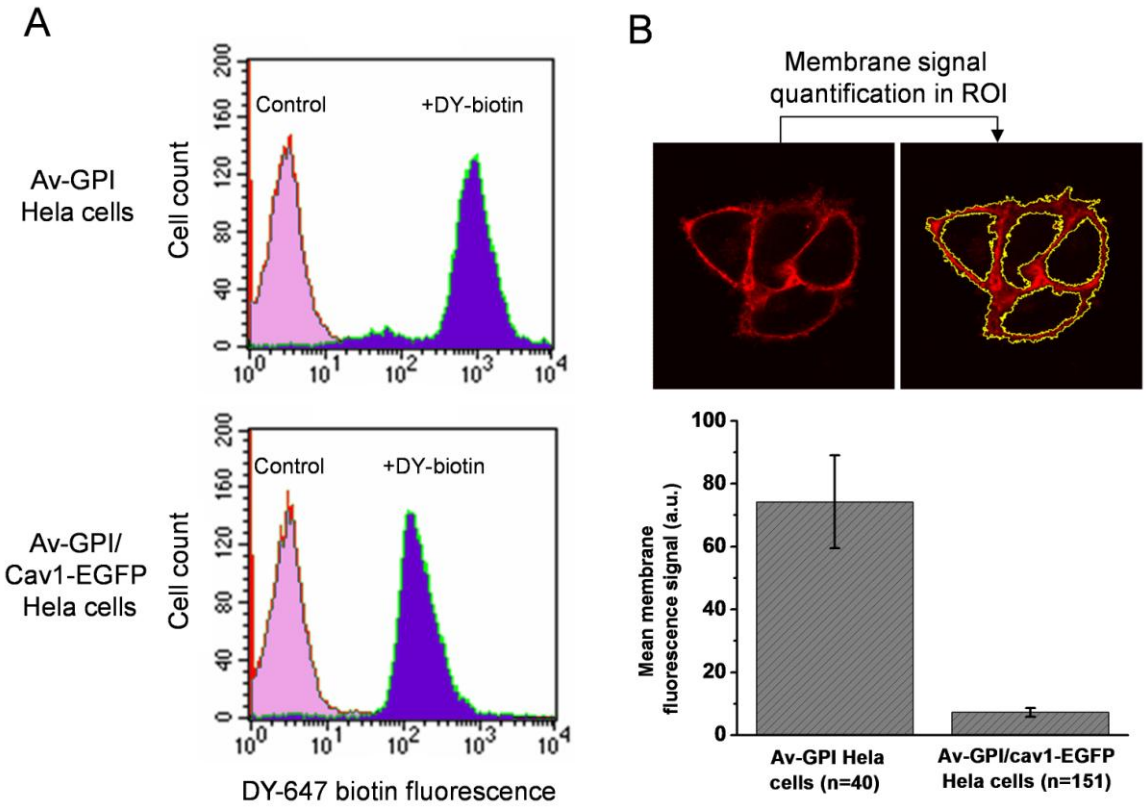

(A) FACS analysis of Av-GPI (top panel) and Av-GPI/Cav1-EGF (bottom panel) expressing HeLa cells after surface labeling with DY-biotin 647 (blue profile) or without labeling (red profile). The surface expression of Av-GPI was about 10 times higher for HeLa cells expressing Av-GPI only.
(B) Quantification of cell surface Av-GPI by confocal imaging confirmed the FACS results and indicated that the amount of membrane-bound Av-GPI was about nearly 10 times higher for HeLa cells expressing Av-GPI only.

Diffusion coefficients and confinement sizes of Av-GPI for various treatments of HeLa cells at room temperature

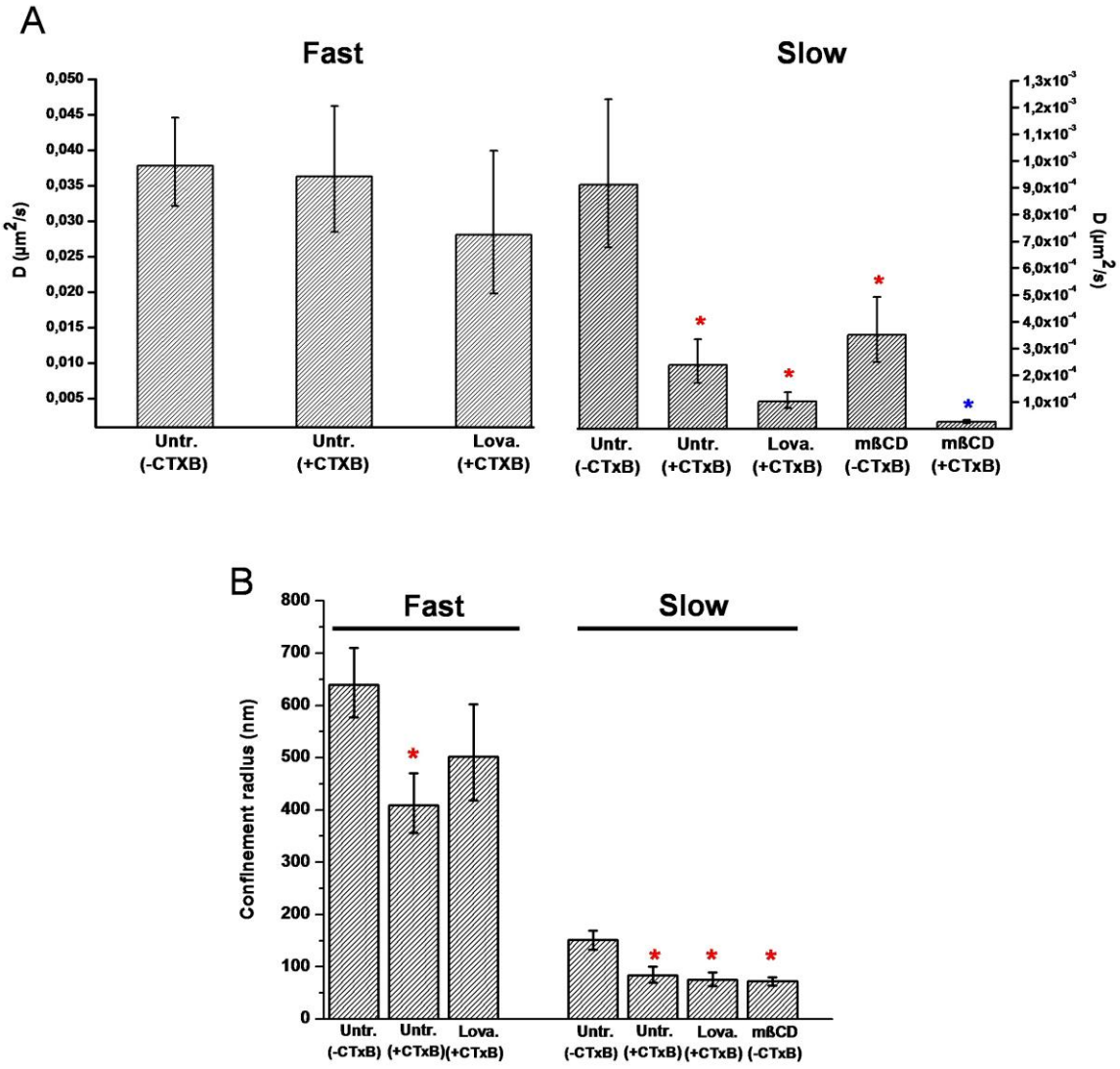

(A) Modal diffusion coefficients of fast and slow distribution of Av-GPI in untreated HeLa cells without (Untr. (-CTxB), 118 Av-GPI, 28 cells), or with CTxB (Untr. (+CTxB), 214 Av-GPI, 19 cells), in cells treated with lovastatin and stained with CTxB (Lova. (+CTxB), 141 Av-GPI, 14 cells), in cells treated with methyl-β-cyclodextrin (mβCD (-CTxB), 52 Av-GPI, 8 cells) and in cells treated with methyl-β-cyclodextrin and stained with CTxB (mβCD (+CTxB), 48 Av-GPI, 11 cells). Red stars indicate significant differences in diffusion coefficient compared to untreated cells (-CTxB). Blue star indicates significant difference compared to untreated and CTxB stained cells (+CTxB) (see Material and Methods). These results are also reported in Table S3.
(B) Confinement size of fast and slow Av-GPI for the same treatments as in (A). Only Av-GPI undergoing restricted diffusion are considered. Definitions for significant differences are the same as in (A).